

Supplement of Atmos. Chem. Phys., 20, 5771–5785, 2020
<https://doi.org/10.5194/acp-20-5771-2020-supplement>
© Author(s) 2020. This work is distributed under
the Creative Commons Attribution 4.0 License.



Supplement of

Mixing characteristics of refractory black carbon aerosols at an urban site in Beijing

Hang Liu et al.

Correspondence to: Xiaole Pan (panxiaole@mail.iap.ac.cn)

The copyright of individual parts of the supplement might differ from the CC BY 4.0 License.

Mixing characteristics of refractory black carbon aerosols determined by a tandem CPMA-SP2 system at an urban site in Beijing

Supplementary

5 **Table S1. Abbreviations and symbols used in this paper**

Abbreviation/symbols	Full name/explanation
SP2	Single particle soot photometer (DMT Technologies)
DMA	Differential mobility analyzer (TSI Inc.)
CPMA	Couette centrifugal particle mass analyzer (Cambustion, Ltd.)
CPC	Condensation particle counter (TSI Inc.)
rBC	Refractory black carbon determined by SP2 through laser-induced incandescence method
D_c	Mass equivalent diameter of rBC core
MMD	Mass median diameter
D_p	Diameter of rBC-containing particles including rBC core and coatings
LEO	Leading-edge-only fitting method
M_p & M_{coat} & M_{rBC}	Mass of rBC-containing particles, mass of coating material, mass of rBC
M_R	M_{coat}/M_{rBC}
D_{mob}	Mobility diameter determined by DMA
ρ_{eff}	Effective density
D_{fm}	Mass fractal dimension
E_{abs}	Absorption enhancement of rBC-containing particles compared to bare rBC
$\sigma_{measured}$	Scattering cross section of rBC-containing particles measured by SP2
σ_{model}	Scattering cross section of rBC-containing particles calculated using the Mie theory

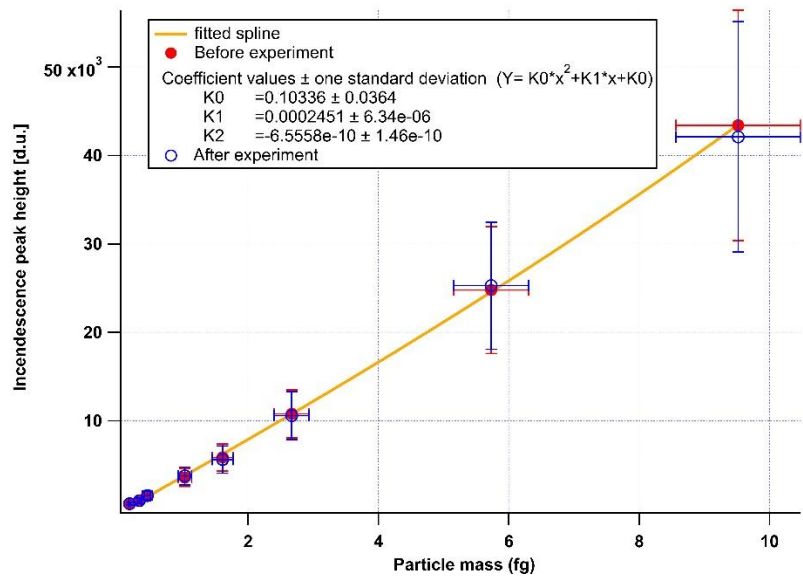
Section 1 Calibration

Figure S1: The calibration of the incandescence channel. The data of incandescence peak and rBC mass
10 is fitted using a poly function ($y = ax^2+bx+c$). The coefficient of the poly function varied little (<2%)
before and after the observation indicating the stability of the incandescence channel. The scatter of
incandescence intensity caused 25% uncertainty, resulting in an uncertainty of the derived BC mass of
20%, which causes an uncertainty of mass equivalent diameter of ~6%.

15 Figure S2: The calibration of the scattering channel. The calibration factor varied little (<3%) before and
after the observation indicating the stability of the scattering channel. The calibration is done using
PSL with multiple sizes (203 nm, 240 nm, 300 nm, 400 nm) before the observation. And the calibration
is done only with PSL with 240 nm after the observation.

20 Figure S3: The calibration curve for the detection efficiency of SP2. For rBC with diameter > 70 nm, the
detection efficiency is larger than 80%.

Figure S4: The calibration of the DMA-SP2 system. An DMA-SP2 system can determine the effective
density of rBC. We test our DMA-SP2 system by measuring the effective density of Aquadag and
25 comparing the result with previous research. Our results are ~7% higher than the poly-fit of Gysel but
lower than the results from Moteki and Kondo. These differences may be result of different
characteristics of Aquadag with varied lot and different instrument condition (such as the uncertainty of
SP2).



30 Figure S1 Calibration curve for incandescence broadband high gain channel.

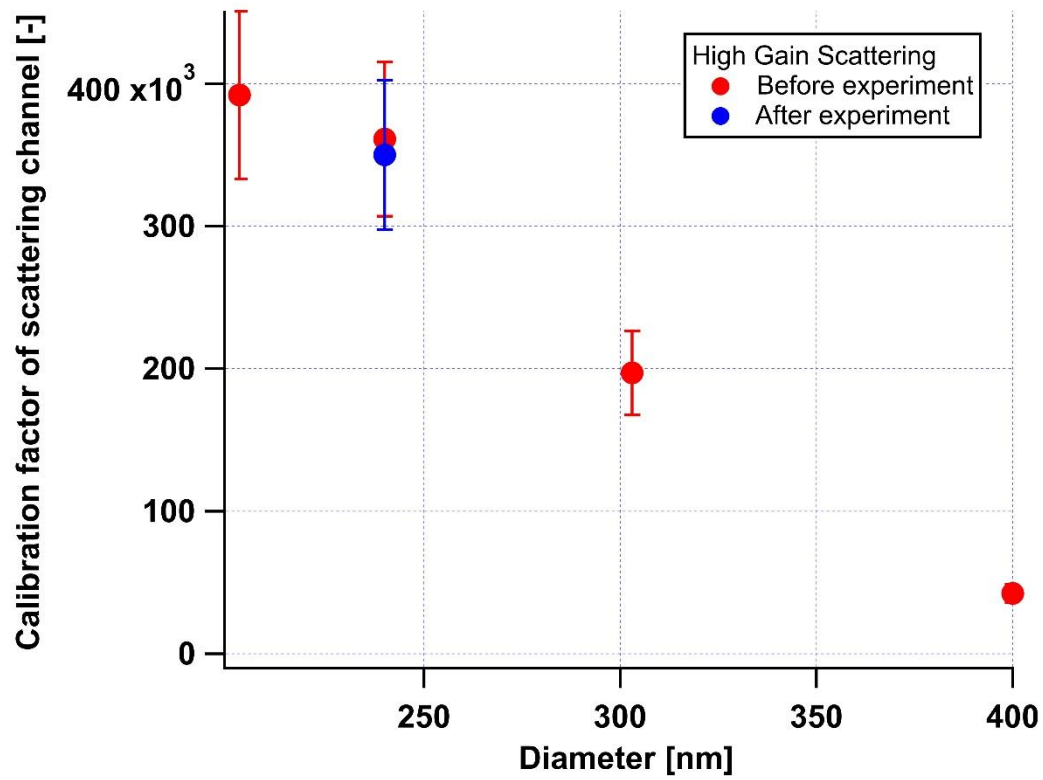
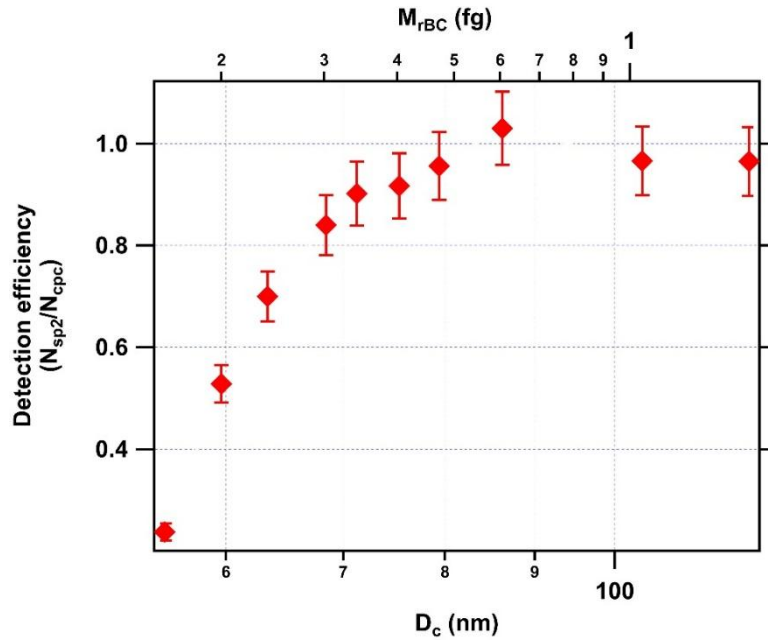


Figure S2 PSL calibration for high gain scattering channel before and after the investigation.



35 Figure S3 Calibration curve for SP2's detection efficiency.

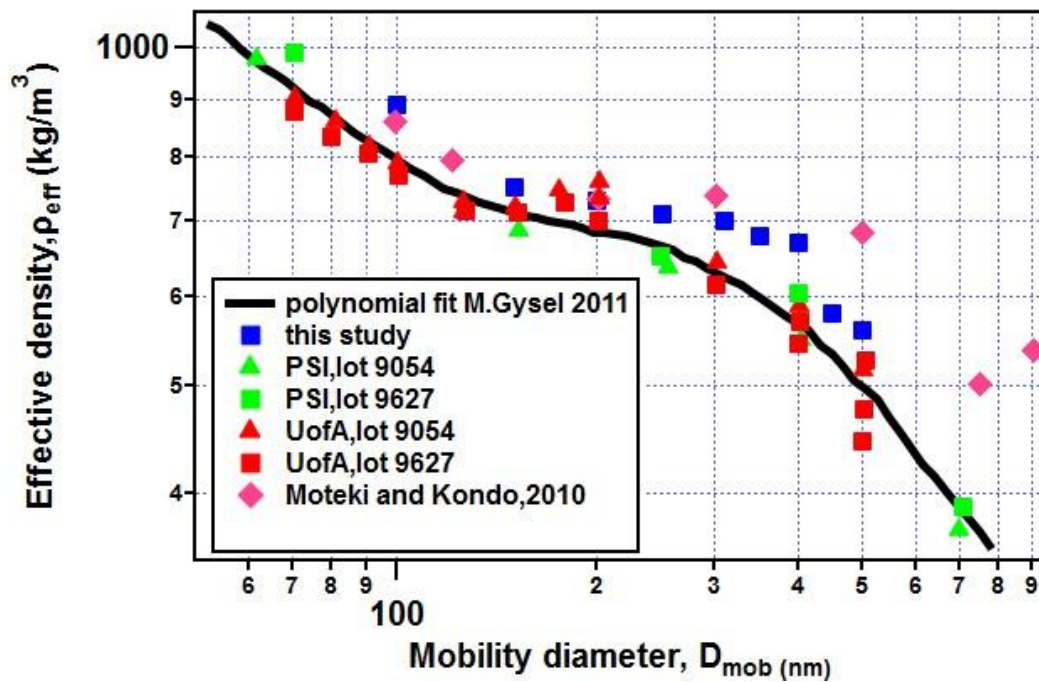


Figure S4 Relationship between effective density and mobility diameter of Aquadag measured in the present study and in previous studies.

40

Section 2 Backward trajectory

An WRF-Flexpart model (<https://www.flexpart.eu>) was used to analyze where the air mass was from. The 1 °*1 °FNL data (rda.ucar.edu/) was used as the input meteorological data to WRF. WRF can produce

meteorological data with higher resolution which was used as the input data for Flexpart. Air samples were released at 100m above ground level at the observation site (longitude: 116.37 E; latitude: 39.97 N) and the simulation time of backward trajectory is 3 days.

On the clean days (06/07, 06/08) the air mass was from the north of Beijing where there is little pollutant emission. Since the north air mass is clean, the local emitted pollutant may be dominant.

On the pollution day (06/12, 06/13), the air mass was majorly from the south polluted area. The pollutant transportation may play an important role in pollution day.

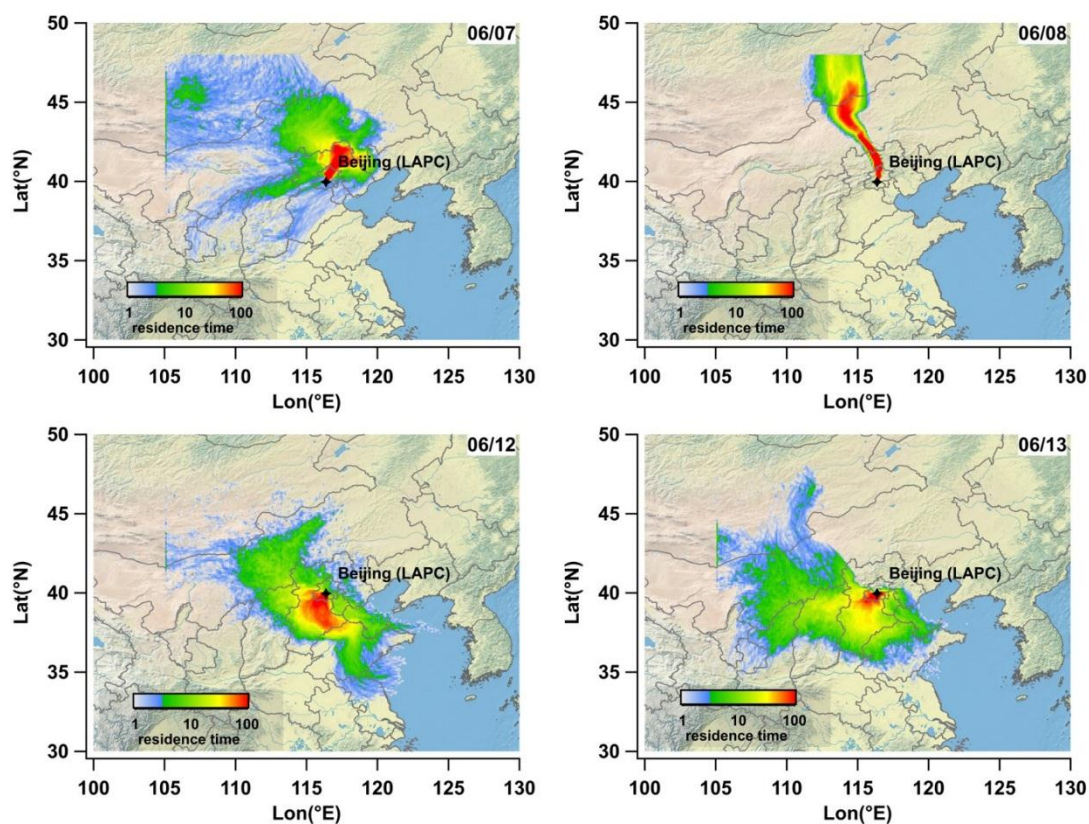


Figure S5 The backward trajectories at clean days (06/07, 06/08) and polluted days (06/12, 06/13), the map is extracted from Igor Pro software (© 2016 wavemetrics, www.wavemetrics.com).

55

Section 3 Absorption enhancement calculation

3.1 Description of morphology-dependent model

The absorption enhancement (E_{ab}) of a single rBC-containing particle is calculated as the ratio of
60 absorption cross section of rBC-containing particle ($C_{abs,p}$) and absorption cross section of rBC core
($C_{abs,rBC}$) using Mie theory assuming a core-shell structure with refractive indices of $2.26+1.26i$ for rBC
core and 1.48 for coatings.

$$E_{abs_coreshell} = \frac{C_{abs,p}}{C_{abs,rBC}}$$

Considering rBC-containing particle is not in an ideal core-shell structure as discussed in section 4.1.2,
65 the rBC-containing particles was classified into external, transition and core-shell stage based on the M_R
range. The rBC-containing particles with an external mixing state were considered to have no absorption
enhancement, and the rBC-containing particles at the core-shell stage were considered to have a core-
shell structure and the same E_{abs} from Mie-theory under the assumption of a perfect core-shell structure.
The E_{abs} in the transition period was calculated by the interpolation of E_{abs} between the external and
70 internal stage, which can be explained as the following equation:

$$E_{abs_new} = \begin{cases} 1 & \text{when } M_R \leq 1.5 \\ \frac{E_{abs_coreshell}(M_R=6) - E_{abs_coreshell}(M_R=1.5)}{6 - 1.5} * (M_R - 1.5) + 1 & \text{when } 1.5 < M_R < 6 \\ E_{abs_coreshell} & \text{when } M_R \geq 6 \end{cases}$$

The reliability of this morphology- dependent model has been proven by comparing the E_{abs} derived from
75 the model and measuring the E_{abs} (Liu et al., 2017).

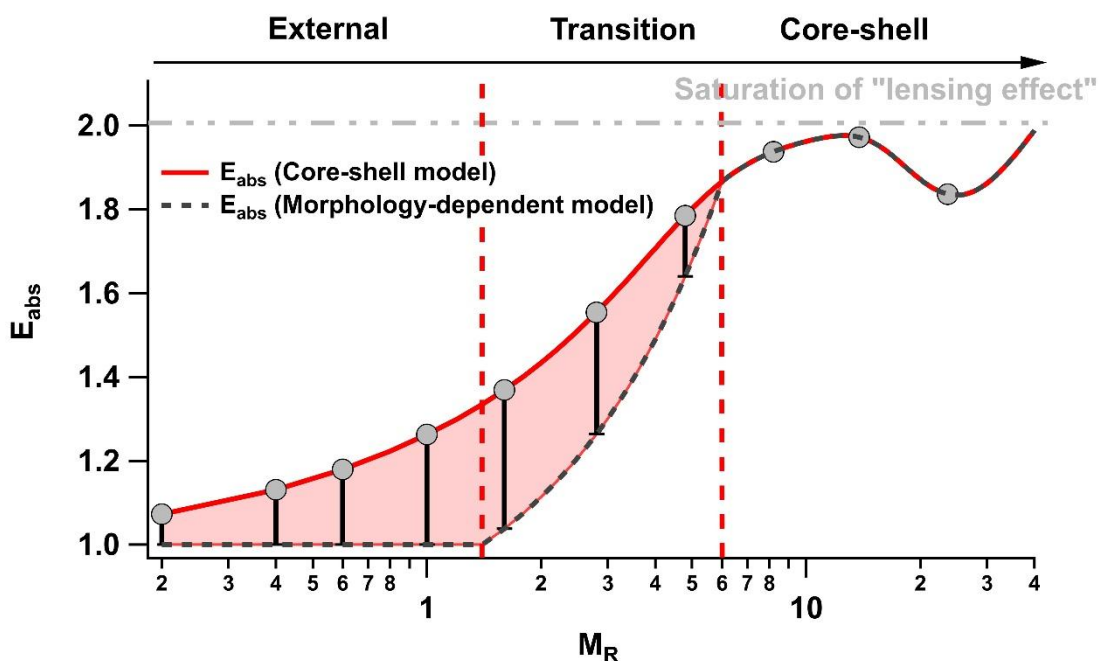
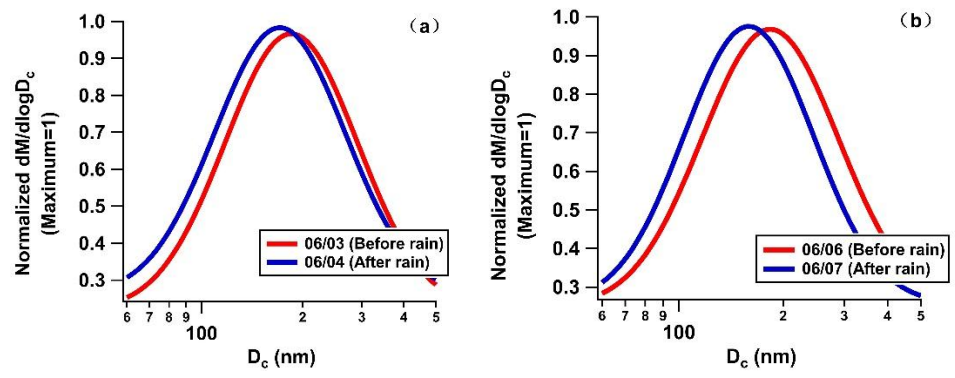


Figure S6 Dependence of E_{abs} on M_R at wavelength of 550 nm and $D_c = 180$ nm, calculated using the Mie model under the assumption of a core-shell structure (red solid line). The gray dashed line denotes the E_{abs} calculated from morphology-dependent model.

3.2 Applying the morphology-dependent model

The D_p and D_c can be directly obtained in the single SP2 measurement. With the rBC density of 1.8 g/cm^3 and assuming a coating density of 1.5 g/cm^3 , the M_R of every single rBC-containing particle can be calculated in the ambient measurement. Thus, the relationship of the morphology-dependent model between M_R and E_{abs} can be used. We calculated the E_{abs} of every single rBC-containing particle with $D_c = 180$ nm in one hour and reported the average E_{abs} in Fig. 12.



90 Figure S7 Size distribution of the rBC core before and after the typical rain cases.